Different sustained and induced alpha oscillations emerge in the human auditory cortex during sound processing

Víctor López-Madrona, Agnès Trébuchon, Christian Bénar, Daniele Schön, Benjamin Morillon

Different sustained and induced alpha oscillations emerge in the human auditory cortex during sound processing

Víctor J. López-Madrona[1,2,#], Agnès Trébuchon[3,4], Christian G. Bénar[2], Daniele Schön[2], Benjamin Morillon[2]

1 Institute of Language, Communication, and the Brain, Aix-Marseille Univ, Marseille, France
2 Aix-Marseille Université, INSERM, INS, Institut de Neurosciences des Systèmes, Marseille, France
3 APHM, Timone Hospital, Epileptology and cerebral rhythmology, Marseille, 13005, France.
4 APHM, Timone Hospital, Functional and stereotactic neurosurgery, Marseille 13005, France.

Corresponding author

ABSTRACT

Alpha oscillations in the auditory cortex have been associated with attention and the suppression of irrelevant information. However, their anatomical organization and interaction with other neural processes remain unclear. Do alpha oscillations function as a local mechanism within most neural sources to regulate their internal excitation/inhibition balance, or do they belong to separated inhibitory sources gating information across the auditory network? To address this question, we acquired intracerebral electrophysiological recordings from epilepsy patients during rest and tones listening. Thanks to independent component analysis, we disentangled the different neural sources and labeled them as “oscillatory” if they presented strong alpha oscillations at rest, and/or “evoked” if they displayed a significant evoked response to the stimulation. Our results show that 1) sources are condition-specific and segregated in the auditory cortex, 2) both sources have a high-gamma response followed by an induced alpha suppression, 3) only oscillatory sources present a sustained alpha suppression during all the stimulation period. We hypothesize that there are two different alpha oscillations in the auditory cortex: an induced bottom-up response indicating a selective engagement of the primary cortex to process the stimuli, and a sustained suppression reflecting a general disinhibited state of the network to process sensory information.

SIGNIFICANCE STATEMENT

Alpha oscillations in the auditory cortex have been associated to functional inhibition, but their anatomical and functional organization is unclear. Here, we compared intracerebral electrophysiological recordings acquired from the auditory cortex of epilepsy patients during rest and pure tones listening, identifying distinct oscillatory and evoked neural sources. Evoked responses are located in the primary cortex, while oscillatory sources are more dispersed. Both exhibit a canonical time-frequency response to auditory stimuli, with a high-gamma increase followed by alpha suppression. Notably, oscillatory sources also present a strong sustain alpha suppression throughout stimulation. These findings underscore the complex interplay of inhibition and information processing in the human auditory cortex, revealing two alpha suppression mechanisms in auditory perception.

INTRODUCTION

The brain is always active, with brain oscillations present even in the absence of any particular stimulus (Buzsaki, 2011; Capilla et al., 2022). Alpha (~10 Hz) oscillations are widely distributed across the cortex and are believed to play a key role in attention, controlling the excitation/inhibition balance and inhibiting the regions nonrelated to the task to gate the information flow between relevant distributed networks (ElShafei et al., 2020; Jensen and Mazaheri, 2010; Klimesch, 2012; Thut et al., 2012). An alpha-like rhythm has been described in the auditory cortex (Lehtelä et al., 1997; Neymotin et al., 2022; Tiihonen et al., 1991), It has a lower frequency than the visual or sensorimotor alpha (6-10 Hz; Armonaite et al., 2022; Frauscher et al., 2018; Groppe et al., 2013), but has been suggested to play an equivalent role, controlling the balance between excitation and inhibition in the auditory cortex (Weisz et al., 2011). However, the anatomical and functional organization of these oscillations is unclear.

During speech processing, alpha activity is suppressed in regions responding to the stimulus, suggesting a local bottom-up disinhibition to favor information processing (Müller and Weisz, 2012; Strauß et al., 2014). On the other hand, alpha activity has also been associated to top-down anticipatory processes (Müller and Weisz, 2012), which may require sources located in higher level areas and to control the excitation/inhibition balance in other regions. In this work, we want to explore the nature and function of alpha sources in the auditory cortex. What are the neural sources of alpha activity, its response profile during auditory stimulation and its relationship with the evoked neural sources processing the sensory input.

Most previous studies were based on non-invasive recordings, which lack the spatial resolution to identify and localize the neural generators of different oscillatory dynamics. Intracerebral recordings in the form of stereotaxic electroencephalography (SEEG) are an excellent approach to characterize the dynamics of the auditory cortex at a millisecond time scale and fine spatial specificity (Liégeois-Chauvel et al., 1994). However, although SEEG electrodes are located directly in the region of interest, each contact may still record the activity from multiple brain sources due to volume conduction. Independent component analysis (ICA) is a methodology that aims to separate the time-courses of the different current generators

contributing to the recorded field potentials (Herreras et al., 2022, 2015; Makarov et al., 2010). It has been extensively used in non-invasive recordings, both to remove artifacts such as cardiac activity or blinks (Jung et al., 2000) and to retrieve neural sources (Chaumon and Busch, 2014; López-Madrona et al., 2022; Velmurugan et al., 2022).

In intracerebral recordings, ICA has the potential to outperform traditional montages (Herreras et al., 2022, 2015). In referential montages, each contact records the activity of both local and remote sources that may be located far away (López-Madrona et al., 2023). One approach is to identify and remove the distant sources, whether it represents the electrical reference (Hu et al., 2007; Whitmore and Lin, 2016), or other neural sources (Michelmann et al., 2018). Moreover, rather than discarding this activity, it is possible to localize and analyze it, similar to the inverse problem in non-invasive recordings (López-Madrona et al., 2023; Medina Villalon et al., 2024). Bipolar montages are commonly used to measure local currents in a given location, but they may not recover the correct time-courses of local sources (Fernández-Ruiz and Herreras, 2013; Martín-Vázquez et al., 2013; Michelmann et al., 2018). For example, if two sources are located close to the same SEEG contact, the bipolar montage would not be able to separate them (López-Madrona et al., 2024). Therefore, ICA can be used to separate the multiple sources of alpha activity in the auditory cortex.

In this work we performed SEEG recordings from the human auditory cortex to track the activity of the neural sources during two conditions: rest and pure tone stimulation. With ICA, we identified the main sources of alpha oscillations at rest ("oscillatory sources") and those with a significant auditory evoked potential (AEP, "evoked sources"). First, we compared whether the sources responding to the stimulus were also those with highest alpha at rest (i.e., whether they were the same neural source or not). Second, we compared the power spectrum across both conditions to characterize sustained changes of alpha power. Finally, we analyzed the time-frequency response of the sources during pure-tone stimulation for a fine-grained exploration of stimulus induced alpha modulations.

METHODS

Participants

A total of 18 patients (10 females) with pharmacoresistant epilepsy were recorded with SEEG during their period of presurgical evaluation at the Hôpital de laTimone (Marseille, France). Neuropsychological assessment carried out before SEEG recordings indicated that all patients had intact language functions and met the criteria for normal hearing. None of them had their epileptogenic zone within the auditory areas as identified by experienced epileptologists. The study was approved in accordance with the Declaration of Helsinki by the Institutional Review board of the French Institute of Health (IRB00003888). Patients provided written informed consent prior to the experimental session. Participation was voluntary, and none of these patients participated in a clinical trial.

SEEG recordings

SEEG recordings were performed using depth electrodes, implanted stereotactically (Talairach et al., 1992; Alcis, Besançon, France, and Dixi Medical, Chaudefontaine, France). All the patients presented, at least, one electrode in the auditory cortex, implanted orthogonally to the cortical surface, recording the tip of Heschl's gyrus, the planum temporale (Figure 1a). From the 18 patients, 5 had bilateral implantations, resulting in a total of 23 analyzed electrodes (N=23). The electrodes had between 8 and 18 contacts per electrode, a diameter of 0.8 mm, 2 mm contact length and separated from each other by 1.5 mm. A scalp electrode placed at Fz was used as reference for the recordings. SEEG signal was recorded on a digital system (Natus Medical Incorporated) with sampling at 1024 Hz with 16-bit resolution, a hardware high-pass filter (cutoff = 0.16 Hz), and an antialiasing low-pass filter (cutoff = 340 Hz). To determine the exact location of each electrode and contact, a co-registration of the postimplantation CT-scan with the preoperative MRI was performed for each patient using GARDEL (Medina Villalon et al., 2018) in-house software (https://meg.univ-amu.fr/wiki/GARDEL:presentation). To compare the contact location across subjects in a common space, the patient specific anatomy was warped using the MNI template (Collins et al., 1994). From the MNI coordinates, we determined in which region was located each SEEG contact using the Brainnetome atlas (Fan et al., 2016).

Implantation and impact of medication

There is no "standard" approach for the electrode implantation, as it is entirely guided by the hypotheses regarding the anatomical location of the epileptogenic zone (EZ). The goal is to identify the specific area for subsequent cortectomy. These hypotheses about the potential location of the EZ are formed based on non-invasive pre-surgical assessments (Phase I), which include a detailed clinical history, surface video-electroencephalographic (EEG) recordings, MRI, and 18FDG-PET scans. Consequently, electrode placement is tailored to each patient's unique clinical profile rather than being standardized.

One of the most commonly explored areas is the perisylvian region, particularly when there is a need to determine whether the patient's epilepsy is temporal, temporo-perisylvian, or purely perisylvian. Misdiagnosing perisylvian epilepsy is a leading cause of surgical failure in temporal epilepsy. Perisylvian epilepsy can be located in various regions, including the insular cortex, frontal operculum, parietal operculum, temporal operculum, and the superior temporal and supramarginal gyri. In this region, electrodes are typically implanted orthogonally to the cortical surface to capture recordings along the electrode from areas like the posterior insula, the tip of Heschl's gyrus, and the planum temporale. Another approach involves implanting electrodes more anteriorly to target the superior temporal gyrus and ventral insula. The perisylvian region is also explored under the hypothesis of epilepsy originating from the inferior parietal lobule, pericentral area, or ventral prefrontal/premotor cortex.

The transverse gyrus (Heschl's gyrus), which includes the auditory cortex, plays a crucial role due to its connections with lower central regions and the inferior frontal gyrus. This region serves as a pathway through which seizures from the temporal pole and the anterior superior temporal gyrus can spread.

Neural recordings were conducted between 4 to 9 days following the implantation procedure, without the use of sedation or analgesic drugs. Typically, antiepileptic drugs are partially or completely withdrawn before the exploration. However, medication levels are adjusted individually based on the type of seizures. Recordings are consistently taken at least 4 hours after the last seizure.

Experimental paradigm

We recorded SEEG activity during rest and a pure-tone stimulation task. The resting condition consisted in three intervals of three minutes each, with the patients sitting awake with eyes closed. The auditory stimuli were composed of 100 pure tone trials, 30 ms long, presented binaurally at 1 kHz. The interval between stimuli was 1.030 (±200) ms. We selected this type of stimulus due to its efficiency to activate the auditory cortex without containing linguistic information (Liégeois-Chauvel et al., 1994). Patients were in a sound-attenuated room while passively listening to the pure tones from loudspeakers. Stimuli were presented using E-prime 1.1 (Psychology Software Tools Inc., Pittsburgh, PA, USA). To facilitate the comparison between conditions, we selected only the first 100 seconds without artifacts during rest, matching with the duration of the auditory task.

Independent Component Analysis

ICA aims to solve the 'cocktail party' problem by separating N statistically independent sources that have been mixed on M recording contacts. While the 'cocktail party' problem is often attributed to the identification of one specific acoustic source among many others, in our case we aim to disentangle the different neural sources generating field potentials (i.e., it is not related to the auditory stimuli). It assumes immobility of the neural sources in space, i.e., that the contribution of one source to the recording contacts is the same throughout the recording session. Each recorded signal $u_m(t)$ is thus modeled as the sum of N independent sources ($s_n(t)$) multiplied by a constant factor (V_{mn}):

$$u_m(t) = \sum_{n=1}^{N} V_{mn} s_n(t)\,, m = 1,2,\dots,M \quad (1)$$

where $u_m(t)$ is the SEEG data, V_{mn} the ICA weights or spatial profile of each source, M the number of contacts, N the number of sources and $s_n(t)$ the obtained independent components ("SEEG-ICs").

We concatenated the time courses of the selected resting condition window and the whole pure tone recording and ran ICA on each electrode (total: 23 electrodes). Thus, each source had a unique spatial profile, allowing a traceability of the activity of the same neural source across conditions. We obtained as many components as available contacts per electrode (N=M), without any prior dimension reduction (Artoni et al., 2018). We used FieldTrip (Oostenveld et al., 2011) to compute ICA based on the infomax algorithm, which aims to minimize the mutual information between components (Bell and Sejnowski, 1995), as implemented in EEGLAB (Delorme and Makeig, 2004). Although not all the SEEG-ICs represented neuronal sources, we did not discard any of them at this point. All the SEEG-ICs were z-scored.

Analysis of auditory evoked potentials (AEPs)

For each SEEG-IC, we checked whether they had a significant AEP during pure tone stimulation. To do so, we tested if each time point across trials was significantly different from zero with a t-test, obtaining a *t*- and *p* values for each time-point. Then, we corrected these tests for multiple comparisons using a local false discovery rate (LFDR; Benjamini and Heller, 2007) on the t-values with a threshold of 0.2 (Pizzo et al., 2019). LFDR assumes that the distribution of t-values is Gaussian, considering as significant those values that stand out from the distribution. To have a better estimation of the distribution, we grouped all the t-values across SEEG-ICs of the same electrode, obtaining a single threshold per electrode. To remove artefactual single points, i.e., single data points that were significant but the anterior and posterior samples were not, we selected only those points during the first second after the stimulus and we imposed a minimum number of consecutive significant time samples (10 ms in this work). No baseline correction was applied during the AEP analysis, as the data was already high-pass filtered (0.16 Hz) and z-scored to remove very low frequency trends.

For each SEEG-IC with a significant response, we selected its activation time as the earliest peak in the AEP (see Figure 4a). This initial peak is generally followed by a much higher response in amplitude. The later response tends to drive the result of most automatic methods, although early activations can be visually detected. Therefore, we used a semi-automatic approach, identifying the local peaks of the AEP using the MATLAB (Mathworks, Natick, MA)

function *findpeaks.m*, imposing a minimum prominence of twice the standard deviation of the AEP during baseline (between -100 ms and 0 ms) and considering both positive and negative peaks. We considered as activation time the first peak identified.

Spectral analysis

Power spectra were estimated using the multitaper method on each SEEG-IC (Thomson, 1982) with a frequency resolution of 0.25 Hz. Then, we followed the *fooof* approach to characterize the power of each source (Donoghue et al., 2020). This methodology separates the periodic and the aperiodic (1/f-like) component of the spectra, allowing the analysis of the oscillatory power independently of the changes in the 1/f distribution (Voytek et al., 2015). The aperiodic component is modeled by a Lorentzian function, where the main parameters are the offset and the exponent (or curvature). Then, the *fooof* method detects each oscillatory peak above the aperiodic components and fits them individually with a Gaussian function, obtaining the power, center frequency and bandwidth of each detected oscillation. We selected the range from 2 to 30 Hz for the *fooof* fit, a minimum bandwidth for peak detection of 0.5 Hz (twice the frequency resolution) and a minimum amplitude of twice the standard deviation of the aperiodic-removed power spectrum (see Supplementary Figure 1 for a distribution of all the identified peaks across SEEG-ICs and conditions). The knee parameter was fixed at zero.

To limit the contribution of the AEPs during pure tone stimulation to the power spectrum, we also analyzed the time-courses after removing the averaged response from each trial (Pure Tone no AEP condition). First, we computed the AEP for each SEEG-IC. This averaged AEP was then fitted for each trial using a linear regression minimizing the difference between the single trial and the fitted AEP and it was subtracted for each trial. In other words, we subtracted to each trial the averaged AEP multiplied by a factor ‘k’ that minimized the result. The remaining time-course should contain all the activity that is not explained by the evoked response. The spectral analysis was computed on the resultant time-course.

Identification of sources (independent components of interest)

We visually inspected all the SEEG-ICs to remove the components related to the reference or to remote sources, i.e., with a similar activity along all the contacts of the electrode (Figure 1d, gray component). Then, we classified the remaining components as "oscillatory" sources if they presented a high alpha oscillatory activity during rest (i.e., a significant peak of power given by the *fooof* analysis), "evoked" sources if they had a significant AEP, both "oscillatory" and "evoked" sources, or "nonrelated" components. A total of 58 SEEG-ICs were labeled as evoked. To determine the oscillatory SEEG-ICs, we selected, for each source, the highest significant peak of the periodic component at 5-10 Hz obtained from the power spectrum during rest. From all the SEEG-ICs, we chose the 25% with highest power (71 SEEG-ICs; 0.75 quantile), labeling them as oscillatory. As one of the goals of this study was to test whether the sources processing the input (i.e., evoked sources) were also the sources with the main alpha oscillatory activity in rest, we fixed this value to include SEEG-ICs from most of the electrodes in the analysis (21 out of 23 electrodes had an oscillatory source) while keeping a similar number of oscillatory and evoked source (71 versus 58, respectively). While the classification of a source as "evoked" is relatively independent of other SEEG-ICs, we determined the "oscillatory" sources given the total number of SEEG-ICs in the analysis. Therefore, we repeated our analysis using quantiles 0.9 and 0.5 to ensure that our selection criterion was not driving the results.

To check that none of the conditions were biasing the resulting SEEG-ICs, we repeated the ICA on each task separately and compared the obtained components with the original sources. First, we performed an ICA and extracted a new set of components for each condition (condition-specific SEEG-ICs). Second, we split the time-courses of the original SEEG-ICs in the two conditions to match the duration of the condition-specific SEEG-ICs. Then, we computed the correlation between the original SEEG-ICs and the condition-specific SEEG-ICs, selecting the maximal correlation, i.e., the most similar component, as it should reflect the same source. Therefore, for each oscillatory and evoked source we obtained two correlation values. One related to the most similar condition-specific SEEG-IC during rest, and another related to pure tone stimulation. If both correlation values are similar and close to 1, it suggests that the same

source is active during both conditions. On the contrary, is the values are maximal in one condition but close to zero in the other, this would indicate that the source is active only during that condition, which would guide the joint analysis.

Time-frequency analysis

In addition to the AEP, we tested whether each SEEG-IC had a response to the pure tone stimulation in the time-frequency plane. We used Morlet wavelets to obtain the time-frequency transformation with 7 cycles per wavelet. Then, the time-frequency responses were averaged across trials for each SEEG-IC and they were baseline corrected using the z-score. The baseline was set between 200 and 300 ms before the stimulus to avoid temporal smearing from post-stimulus activity.

To compute the statistical differences with baseline at the group level, either across oscillatory SEEG-ICs or evoked SEEG-ICs, we performed a surrogate analysis followed by a cluster-based correction (Cohen, 2014; Maris and Oostenveld, 2007). First, we selected the averaged response of each SEEG-IC and we computed a t-test across sources between each time-frequency point after the stimuli against the baseline at the same frequency. We defined a cluster of significance as a group of adjacent time-frequency points with a significant p-value (non-corrected p-value lower than 0.01 in this work). We assigned to each cluster the sum of the t-values within the cluster (either positive or negative). For each surrogate (N=1000), we randomly shifted the time of the stimuli in a window of ±500 ms around the original value. This way, the time-frequency response remained the same, but the temporal alignment was broken. We repeated the cluster procedure for each surrogate, keeping both the clusters with maximal and minimal t-value at each iteration. Any significance found in these surrogates would be by chance. Finally, we tested whether the t-values of our original clusters were significantly higher than the maximal t-values of the surrogate analysis for positive effects or lower than the minimum for negative effects. The threshold of significance was set at the 97.5 percentile of the distribution of surrogate values (p-value < 0.025), including the observed value into the simulated values to avoid p-values equal to zero (Phipson and Smyth, 2010).

The statistical comparison of the time-frequency responses of the oscillatory SEEG-ICs versus the evoked the SEEG-ICs was performed using a t-test. We computed the statistical test across sources between each time-frequency point of the oscillatory SEEG-ICs and the same point of the evoked SEEG-ICs. Then, we corrected all the p-values using FDR.

As a single patient may have several SEEG-ICs and, therefore, drive the results, we repeated the time-frequency analysis averaging, for each subject, all the oscillatory or evoked sources. This way, only one averaged oscillatory source and one evoked source were considered in the analysis, obtaining a number of observations equal to the number of participants with, at least, one significant oscillatory or evoked SEEG-IC.

Inter-trial phase clustering

We analyzed how much of the time-frequency activity was related to the presence of the AEP using the inter-trial phase clustering (ITPC; Cohen, 2014). For each time point and frequency, it measures the distribution of phases across trials as:

$$ITPC(t,f) = \left| \frac{1}{N} \sum_{n=1}^{N} e^{i\varphi_{ntf}} \right| \quad (2)$$

where φ_{ntf} is the phase of the signal at trial n, time t and frequency f. If the distribution is centered around a specific phase, i.e., it is consistent across trials, then the ITPC value would be close to one. On the hand, a uniform distribution would yield an ITPC value close to zero.

We also tested whether the instantaneous phase at stimulus arrival conditioned the brain response (Krieg et al., 2011): either the amplitude of the AEP or the changes of power at high gamma (80-120 Hz) and alpha (5-10 Hz) frequencies. To do so, we used a weighted ITPC (wITPC):

$$wITPC = \left| \frac{1}{N} \sum_{n=1}^{N} b_n e^{i\varphi_{\alpha n}} \right| \quad (3)$$

where $\varphi_{\alpha n}$ was the alpha (6-10 Hz) phase at stimulus arrival for the trial n, and b_n were the different factors to test (amplitude of the AEP, gamma and alpha power).

The amplitude of the AEP for each trial was obtained from the linear model used to remove the contribution of the evoked response (factor 'k', see *Spectral analysis* section). The gamma power was obtained as the maximal value in the time-frequency map of each trial, using a time from 0 to 200 ms, and a frequency bandwidth from 80 to 120 Hz. The same approach was followed for the alpha power, but selecting the minimum value (i.e., the highest alpha suppression) in the time window from 100 to 300 ms and the frequency band from 0 to 20 Hz.

The statistical analysis of the wITPC was done using permutation testing (Cohen, 2014). On each iteration (n=1000) the b_n values were randomly distributed across trials breaking the relationship between phases and factors and creating a null hypothesis distribution. Then the z-scored of the measured wITPC is computed by subtracting the mean of the null hypothesis and then dividing by the standard deviation. Finally, z-scored wITPC values higher than 1.96 (95% confidence interval) were considered significant.

Onset latency of gamma activity

We measured the event-related gamma power by averaging, for each trial, the baseline corrected time-frequency map between 80 and 120 Hz, obtaining a single time course for each SEEG-IC. Then, we computed whether this activity was significantly different from zero following the same approach as for the auditory evoked potentials. Finally, the onset latency of each source was considered as the first time point of the event-related power significantly different from zero and with a minimal duration of 30 ms (Nourski et al., 2022).

Statistical analysis

To compare whether the location of the oscillatory and evoked SEEG-ICs is different, we selected for each source its location on the x-axis (lateral-medial axis) using the MNI coordinates. This dimension was selected as it corresponds to the trajectory of the implanted

electrodes, allowing a good sampling from medial to lateral locations and intra-electrode comparisons. First, we compared with a t-test whether the absolute values of the coordinates were different between sources. Then, we measured whether the location of the sources was distributed or local by computing the variance of the location in the lateral-medial axis. A large variance would indicate that the sources are distributed along the axis, while a small value would suggest that the sources are located in a specific location. We tested whether the standard deviation of the location in the oscillatory SEEEG-ICs was different from the evoked SEEG-ICs using a permutation test. For each of n=1000 permutations, we randomly labeled each SEEG-IC as oscillatory or evoked, preserving the original ratio. We then computed the difference between the standard deviation of the location of the permuted oscillatory SEEG-IC and the permuted evoked SEEG-IC. Finally, we counted on how many permutations the obtained difference was higher than the original value. This value was divided by the total number of permutations plus the observed value (n=1001) to obtain the p-value (Cohen, 2014; Phipson and Smyth, 2010).

To test how the dynamics of the same SEEG-IC vary across conditions (rest versus pure tone), we tested different features of the power spectrum (peak frequency, relative power and aperiodic component) using a paired t-test. To test whether the different features vary across the lateral-medial axis of the auditory cortex, we computed the Pearson correlation between the x coordinates of each sources and the value of the different features.

RESULTS

Separation of resting and auditory sources with ICA

We recorded the SEEG activity from the auditory cortex (Figure 1a) of 18 epileptic patients during rest and during the presentation of pure tones (Figure 1b and 1c). We selected a total of 23 electrodes (5 patients having a bilateral implantation), each with multiple channels (between 8 and 18, total channels: 305). For each electrode, the time courses of both conditions were concatenated, and the ICA source separation method was applied to segregate the recordings into the main neural sources contributing to the SEEG activity (Figure 1d). A single mixing matrix (i.e., a set of spatial profiles) was obtained for each electrode, allowing traceability of the same sources across both conditions (Figure 1e and 1f). After removing the components associated to remote sources (Figure 1d, gray component), a total of 284 SEEG independent components (SEEG-ICs) were selected across electrodes. We then classified each SEEG-IC as oscillatory source, evoked source, both oscillatory and evoked source or nonrelated component (see methods). A total of 58 SEEG-ICs presented a significant auditory evoked potential (AEP; N=23/23 electrodes) and were, therefore, labeled as evoked, while 71 SEEG-ICs were labeled as oscillatory (N=21/23 electrodes). Interestingly, from all the SEEG-ICs, only 11 were labelled as both oscillatory and evoked, suggesting that the neural sources with the main oscillatory activity in rest were not the sources processing the stimulus (they did not have a significant AEP).

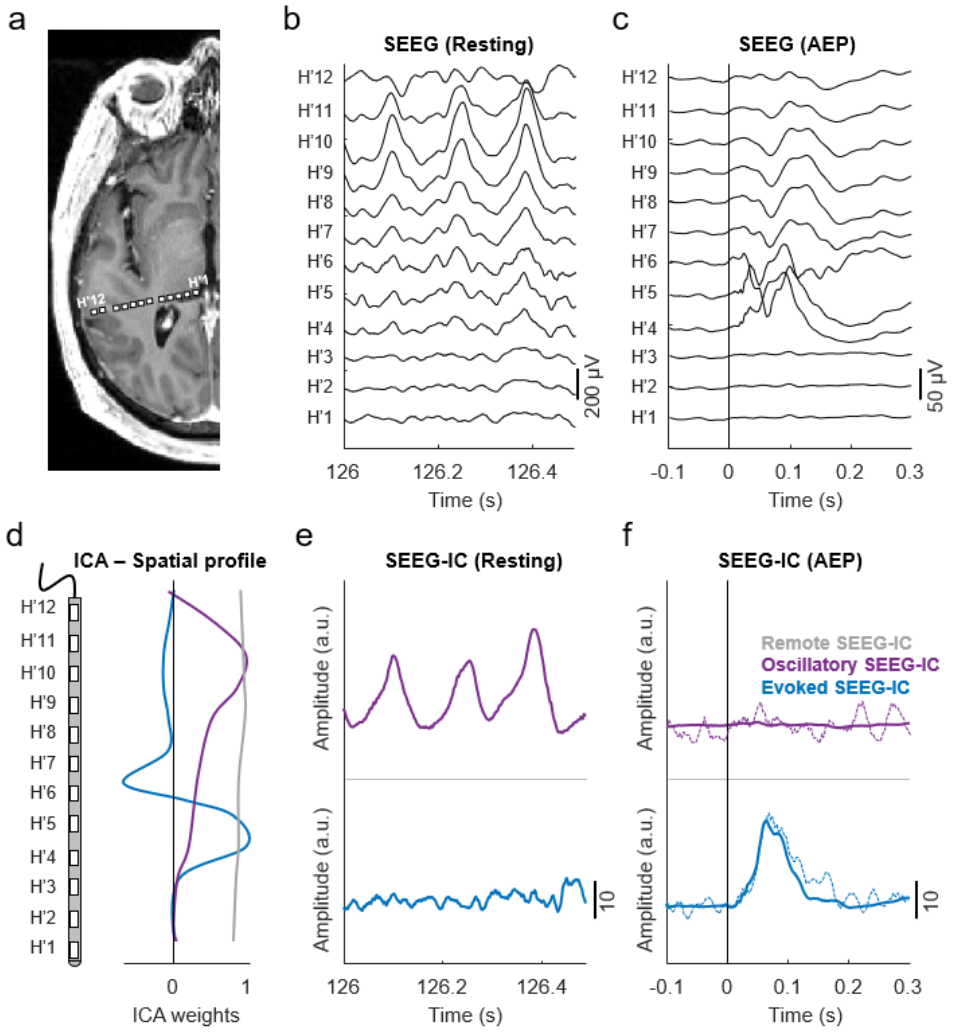

Figure 1: Separation of oscillatory and evoked sources with ICA:

a) Cerebral MRI scan (3D T1-weighted) – cross section with reconstruction of the SEEG electrode for patient 9. The location of each contact is represented with white rectangles.

b) Example of monopolar recordings during rest. High amplitude oscillations can be appreciated in the superior channels (H'9 and H'10).

c) Averaged AEP during presentation of pure tones at each contact. The highest response in amplitude is observed in channel H'4.

d) Spatial profile of three SEEG-ICs across the electrode, representing their contribution to each contact. The purple and blue components have clear peaks in the profile, suggesting a local origin of the sources around these contacts. The grey component contributed almost equally to all the contacts, and hence reflect a remote source.

e) SEEG-IC traces during the same time period as panel b. The oscillations visible in the raw SEEG were captured by the purple component, which was labeled as oscillatory source.

f) Averaged AEP of each SEEG-IC (solid lines) and a single trial (dashed lines). Only the blue component has a significant response and was labeled as evoked source.

The explained variance of the SEEG-ICs (i.e., contribution of the component to all the SEEG recordings) were different for both sources. Each oscillatory source explained between 0.4% and 63% (mean 10.5%) of the total activity of the data, while evoked sources captured between 0.4% and 27.5% (mean 6.4%) of the variance, suggesting that spontaneous activity was predominant in our recordings.

To further check that the obtained sources were not driven solely by one of the two conditions, we repeated the ICA procedure on each condition separately and computed the correlation between the previous SEEG-ICs (with both conditions concatenated) and the new time courses (computed separately for both conditions; see methods). The oscillatory components were quite stable across analyses, and the same components were retrieved when ICA was computed only on the rest condition (averaged correlation of SEEG-ICs ± standard deviation, s.d.: 0.84 ± 0.13) or only during the stimulation condition (0.84 ± 0.14). Results were similar for the evoked sources, although it was more difficult to retrieve them when analyzing only the rest condition (averaged correlation of SEEG-ICs: 0.76 ± 0.13), compared to the pure tone condition (0.81 ± 0.15). Therefore, the two types of sources were present at both rest and during stimulation, rather than being active only in one condition and completely silent during the other.

The location of the SEEG-ICs differed for both types of sources (average of absolute lateral-medial axis locations in MNI space ± s.d.: 50.39 ± 11.65 and 43.49 ± 8.89 for oscillatory and evoked SEEG-ICs; p=0.0024, t-test, t=3.09, df=125; Figure 2a), with evoked sources located in medial areas while oscillatory sources were more lateral. The contacts with maximal contribution of the oscillatory SEEG-ICs were distributed along the lateral-medial axis, in contrast to the evoked sources, which were clustered in more medial areas (Figure 2b). The oscillatory sources occupied a larger area (i.e., they were more distributed) than the evoked sources, with their location presenting a higher standard deviation across SEEC-ICs (s.d. of the absolute lateral-medial axis locations in MNI space: 11.65 and 8.89 for oscillatory and evoked SEEG-ICs, p=0.03, permutation test).

Regarding the anatomical region of each SEEG-IC (table 1), the oscillatory sources were predominately located in the Superior Temporal Sulcus (STS) and the areas 22 and 41/42 of the Superior Temporal Gyrus. The evoked sources were mainly in the STG (areas TE1.0 and TE1.2; primary auditory cortex (Morosan et al., 2001)) and the insular gyrus. None of the evoked SEEG-ICs were identified in the STS.

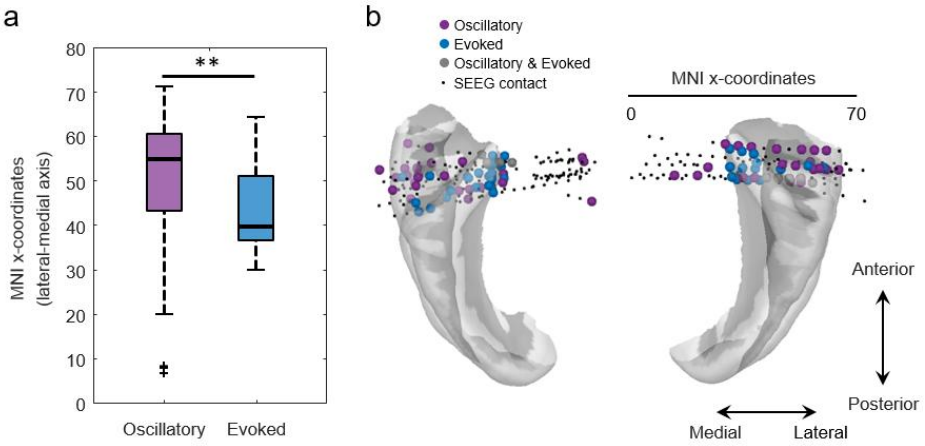

Figure 2: Location of oscillatory and evoked SEEG-ICs:

a) Comparison of the location of oscillatory and evoked SEEG-ICs along the lateral-medial axis, grouping both hemispheres (i.e., absolute value of the x-axis in MNI space; ** $p<0.01$, t-test). The central mark of the box indicates the median, and the bottom and top edges of the box indicate the 25th and 75th percentiles. The whiskers extend to the most extreme data points not considered outliers, and the outliers are plotted individually with black crosses.

b) Position of the SEEG-ICs on a 3D surface of the temporal lobe. The location of each SEEG-IC in a common MNI space is measured as the contact with maximal contribution in the spatial profile.

Region	# Oscillatory SEEG-ICs	# Evoked SEEG-ICs
STG (A41/A42)	13	8
STG (A22c)	7	3
STG (A22r)	4	3
STG (TE1.0 and TE1.2)	5	11
STS (cpSTS)	6	**0**
STS (rpSTS)	6	**0**
Insular gyrus	3	13
Other	16	9
Total:	**60**	**47**

Table 1: Anatomical location of each SEEG-IC. STG: Superior Temporal Gyrus; A22c: caudal area 22; A22r: rostral area 22; STS: Superior Temporal Sulcus; cpSTS: caudoposterior STS; rp: rostroposterior STS.

Resting oscillations are attenuated during pure tone stimulation

To further characterize the dynamics of the oscillatory SEEG-ICs, we analyzed their relative power spectrum, by removing the aperiodic activity following the *fooof* approach (Donoghue et al., 2020; Figure 3a; see methods). All the SEEG-ICs labeled as both oscillatory and evoked were removed from the analysis (resulting in N=60 purely oscillatory ICs). For each purely oscillatory SEEG-IC, we measured the frequency and relative power of its main oscillatory activity and the exponent and offset of the aperiodic component of its power spectrum (Figure 3b). The frequencies of the oscillations were relatively narrow, ranging between 5 and 10 Hz (frequency peak: 7.9 ± 1.04 Hz and 8.1 ± 1.4 Hz, mean ± s.d. for rest and pure tone conditions), with no differences between rest and pure tone stimulation (paired t-test, $p>0.15$, $t=-1.48$, $df=59$, CI=-0.58, 0.09, effect size=-0.25; Figure 3c). Since frequency resolution can impact the quality of the fit in the FOOOF algorithm, we repeated the analysis with a higher resolution (0.05 Hz; original resolution = 0.25 Hz; see Methods) with equivalent results (frequency peak: 7.9 ± 1.06 Hz and 7.9 ± 1.09 Hz, mean ± s.d. for rest and pure tone conditions; paired t-test, $p>0.7$, $t=-0.38$, $df=59$, CI=-0.08, 0.06, effect size=-0.01). However, the relative power of the oscillatory activity strongly decreased during the pure tone condition (1.04 ± 0.23 arbitrary units, a.u., and 0.67 ± 0.32 a.u. for oscillatory SEEG-ICs during rest and stimulation; paired t-test, $p<0.001$, $t=8.23$, $df=59$, CI=0.28, 0.46, effect size=0.37; Figure 3d), suggesting an interruption of the cortical rhythmicity during listening. The aperiodic features also presented slight differences, with higher values during rest (exponent: 1.73 ± 0.48 a.u. and 1.65 ± 0.41 a.u. for oscillatory SEEG-ICs during rest and stimulation; paired t-test, $p=0.0095$, $t=2.68$, $df=59$, CI=0.02, 0.14, effect size=0.08; offset: -0.27 ± 0.40 a.u. and -0.43 ± 0.45 a.u.; paired t-test, $p<0.001$, $t=3.54$, $df=59$, CI=0.07, 0.25, effect size=0.16), indicating a steeper slope during the resting condition.

Then, we tested whether the dynamics of the oscillatory SEEG-ICs were dependent of their location within the auditory cortex, computing the correlation between the spectral features of the sources and their anatomical location in MNI coordinates along the lateral-

medial axis (same direction as the electrode). Although the oscillatory sources covered a relatively broad section in this axis, we could not identify any gradient between the analyzed features and the location (Supplementary Figure 2), suggesting that oscillatory dynamics are independent of the depth of the neural source.

Although the oscillatory SEEG-ICs did not have a significant AEP during pure tone stimulation, they presented significant responses in the time-frequency domain (Figure 3e). An initial response was elicited at low gamma frequencies (20-40 Hz; 25-100 ms), followed by a high-gamma activation (80-120 Hz) that lasted from 50 to 150 ms after stimulus onset ($p<0.05$, corrected with FDR). This increase of activity was followed by a suppression at low frequencies between 5 and 30 Hz that started at 200 ms. To test that a single patient with several SEEG-ICs was not driving the results, we repeated the analysis by averaging all the oscillatory sources per subject (number of observations equal to the number of patients with an oscillatory source), obtaining the same time-frequency pattern (Supplementary figure 3).

To ensure that the results were not driven by our selection criteria of oscillatory sources (25% of SEEG-ICs with highest oscillatory power), we repeated the analysis selecting the 10% and 50% of SEEG-ICs with highest power. We found similar significant differences in relative power across conditions and similar time-frequency responses to pure tones in both cases (results not shown).

Xº

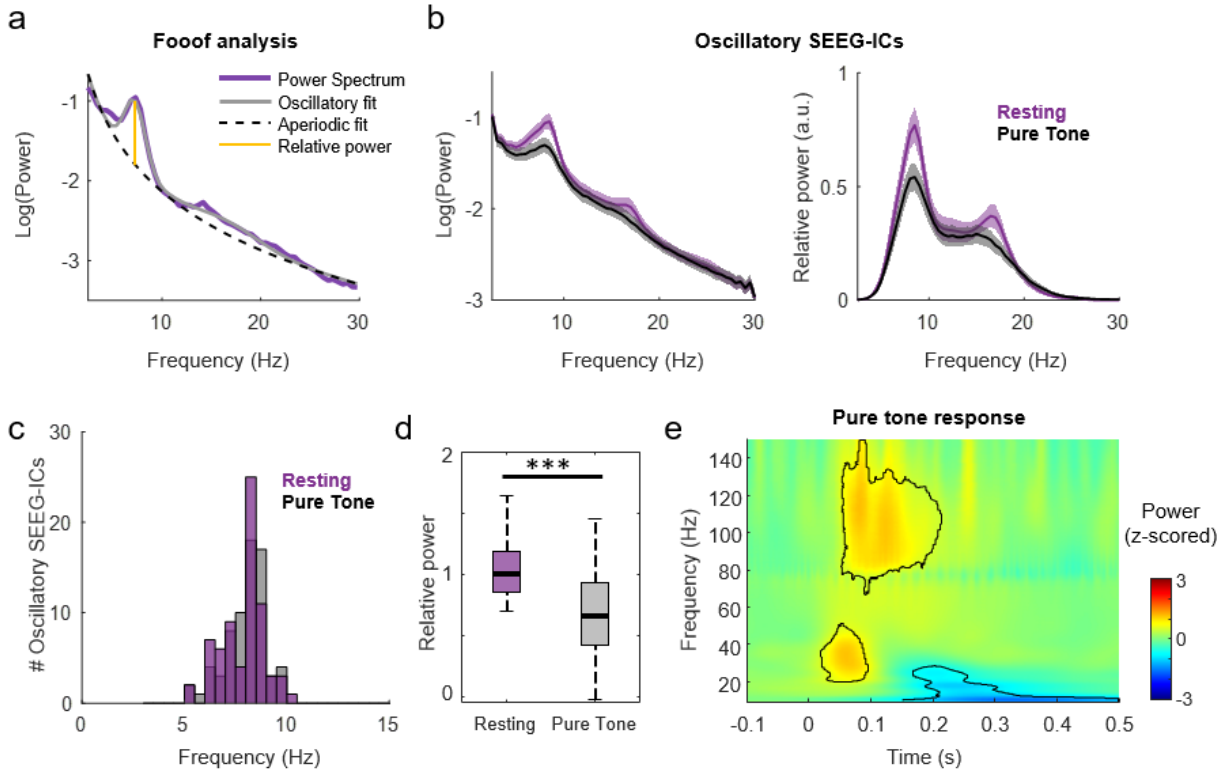

Figure 3: Dynamics of oscillatory SEEG-ICs during rest and pure tone stimulation:

a) Scheme of the *fooof* approach. The power spectrum of a SEEG-ICs is modeled by the combination of the oscillatory sources and an aperiodic activity. The relative power of an oscillatory rhythm is then measured as the difference between both sources (red line).
b) On the left, averaged power spectrum across oscillatory SEEG-ICs during rest and pure tone stimulation (N=60, mean ± s.e.m.). On the right, relative power of the oscillatory SEEG-ICs during both conditions, measured as the difference between the oscillatory and the aperiodic fit.
c) Histogram of main frequency peaks of the oscillatory sources during rest and pure tone stimulation.
d) Comparison of the relative maximal power of the oscillatory SEEG-ICs obtained with the *fooof* approach between conditions (*** p<0.001).
e) Time-frequency response of the average oscillatory SEEG-ICs during pure tone stimulation. Framed areas represent clusters of significant modulation of activity compared to baseline (-300 -200 ms; p<0.01, surrogate analysis).

Medial sources are activated earlier than lateral sources during pure tone stimulation

We then characterized the dynamics of the evoked SEEG-ICs by analyzing the latencies of their evoked potentials (Figure 4a). All the SEEG-ICs labeled as both oscillatory and evoked were removed from the analysis (resulting in N=47 purely evoked ICs). There were a large variety of responses, scaling from 15 to 80 ms after stimulus onset and including positive and negative

patterns. We focused on the earliest latency of each SEEG-IC as an indicator of its activation time (Figure 4a). This response correlated with the SEEG-IC location in the lateral-medial axis (Figure 4b, Pearson correlation, R=0.336, p=0.021, t=2.396, df=45). The first SEEG-ICs responding to the stimulus were in the deeper areas of the auditory cortex, followed by a sequential activation of SEEG-IC sources in the lateral direction (Figure 4c).

As for the oscillatory SEEG-ICs, we analyzed the spectral content of the evoked SEEG-ICs (Figure 4d). To control for the contribution of the AEPs to the power spectrum, we measured the power spectrum either on the raw signal (Figure 4d, Pure Tone) or after removing the averaged evoked response (AEP; i.e., the phase-locked activity) from each trial. We then estimated their relative power with the *fooof* approach (Figure 4d, Pure Tone no AEP; see methods). First, the relative alpha power in these evoked sources was minimal compared to the oscillatory SEEG-ICs (evoked: 0.20 ± 0.20 a.u.; oscillatory: 1.04 ± 0.23; in the Resting condition). Then, the relative alpha power was apparently higher during rest than pure tone (0.20 ± 0.20 a.u. and 0.17 ± 0.15 a.u. for evoked SEEG-ICs during rest and stimulation; paired t-test, p=0.009, t=2.75, df=46, CI=-0.014, 0.094, effect size=0.05; Figure 4e, left). However, this effect was induced by the AEP, as it was not present after removing the phase-locked activity (Resting vs. Pure Tone no AEP: 0.20 ± 0.20 a.u. and 0.19 ± 0.17 a.u. for evoked SEEG-ICs during rest and stimulation without AEP; paired t-test, p=0.69, t=0.397, df=46, CI=-0.05, 0.07, effect size=0.01). This indicates that in these evoked neural sources, alpha oscillatory activity does not vary between rest and stimulation.

The aperiodic features were also strongly driven by the AEP (Figure 4e). Both the exponent and the offset were apparently higher during pure tone stimulation than rest (exponent: 1.24 ± 0.38 a.u. and 1.54 ± 0.42 a.u. for evoked SEEG-ICs during rest and stimulation; paired t-test, p<0.001, t=-5.03, df=46, CI=-0.30, -0.13, effect size=-0.21; offset: -0.59 ± 0.37 a.u. and -0.20 ± 0.39 a.u., paired t-test, p<0.001, t=-5.16, df=46, CI=-0.44, -0.19, effect size=-0.32). However, after removing the effect of the evoked response (AEP), we observed the opposite effect, similar to what was found for the oscillatory sources, with significantly higher values during rest, indicating a steeper slope in the resting condition (exponent: 1.24 ± 0.38 a.u. and 1.05 ± 0.29 a.u. for evoked SEEG-ICs during rest and stimulation without AEP; paired t-test,

p<0.001, t=5.20, df=46, CI=0.11, 0.26, effect size=0.18; offset: -0.59 ± 0.37 a.u. and -0.83 ± 0.29 a.u., paired t-test, p<0.001, t=5.18, df=46, CI=0.15, 0.34, effect size=0.24). Of note, no correlation was found between the location of the sources in the lateral-medial axis and the main features of the power spectrum during the stimuli: relative power, exponent and offset of the aperiodic activity (Supplementary Figure 2).

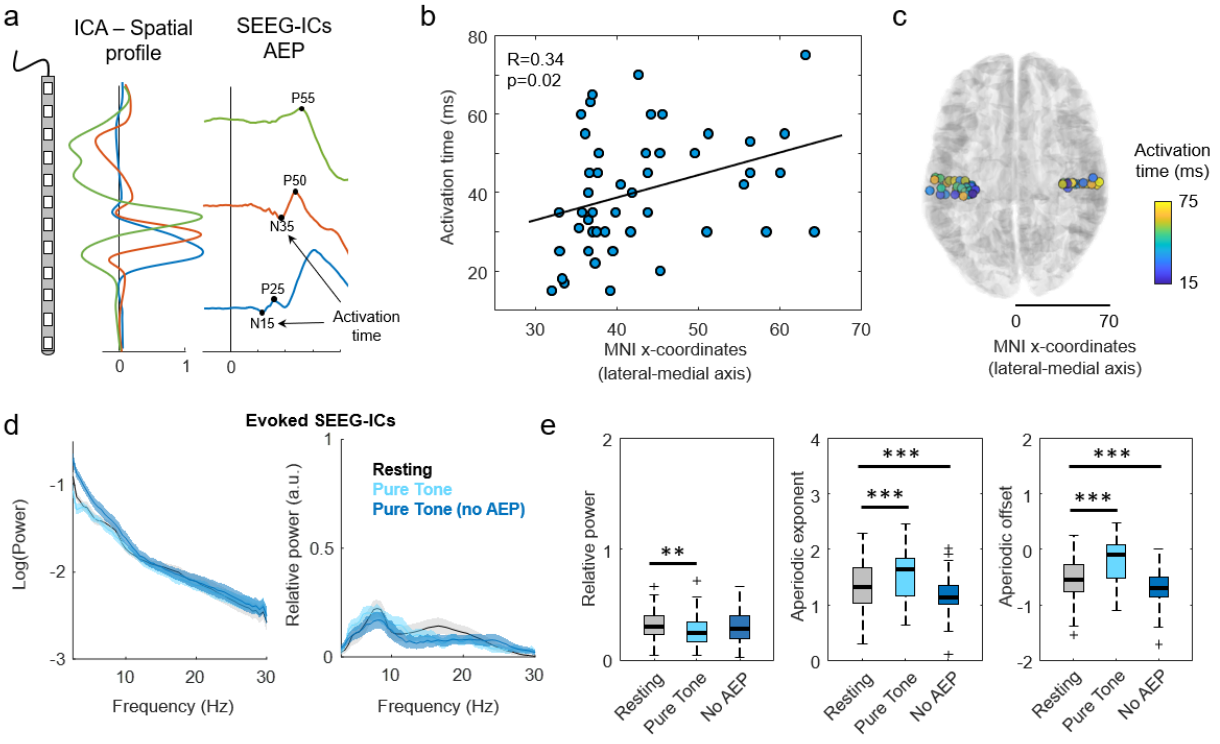

Figure 4: Dynamics of evoked SEEG-ICs during rest and pure tone stimulation:

a) Example of evoked SEEG-ICs in patient 4. The source with the most medial topography (i.e., peak of the spatial profile in deeper contacts) has a faster activation time (blue trace).

b) Pearson correlation (black line) between the location of the evoked SEEG-ICs in the lateral-medial axis and the activation time (blue circles).

c) Location of the evoked SEEG-ICs in a common MNI space. The color of each circle indicates the activation time of the source located in that location.

d) On the left, averaged power spectrum across evoked SEEG-ICs during rest and pure tone stimulation, either including or removing the contribution of the AEP to the time-course (N=47, mean ± s.e.m.). On the right, relative power of the evoked SEEG-ICs for each condition.

e) Comparison of three features extracted with the fooof approach for each condition: relative power (left panel), exponent of the aperiodic component (middle) and offset (right; **/***, pval < 0.01/0.001, respectively; paired t-test).

Induced alpha responses are equivalent between oscillatory and evoked sources

The time-frequency response of the evoked SEEG-ICs was also driven by the AEP (Figure 5). The waveform of the auditory response had a ~10 Hz pattern and most of the activity at low frequencies was strongly phase-locked with the stimulus (Figure 5a, right panel). The AEP also created a chimney effect in the time-frequency spectrum, close to stimulus onset. Therefore, neural activity in the entire frequency range was affected by the AEP and cannot be directly associated with changes in the oscillatory dynamics. To mitigate this effect, we also analyzed the response after removing the averaged evoked response (AEP; i.e., the phase-locked activity) from each trial (see Methods). Without the AEP contribution, the time-frequency map of the evoked sources had some similarities with the oscillatory sources (Figure 5b vs. Figure 3e). There was an early activation (here at very low frequencies; ~10 Hz) with a strong high-gamma response that started 25 ms after stimulus onset and lasted 200 ms, followed by a suppression at low frequencies (between 5 and 30 Hz), starting at 125 ms in these sources ($p<0.05$, corrected with FDR). We repeated the analysis by averaging all the evoked SEEG-ICs per subject (number of observations equal to the number of patients with an evoked source), obtaining the same time-frequency pattern (Supplementary figure 3).

As the frequency of the AEP waveform overlapped with the alpha range, we could not dissociate whether the phase-locked activity was also contributed by a phase resetting of the ongoing oscillations. To better explore this scenario and knowing that the phase of ongoing oscillations in auditory cortex likely modulates its responsiveness to incoming stimuli (Ahveninen et al., 2024; Schroeder et al., 2008; Thézé et al., 2020), we measured how the instantaneous phase of alpha at stimulus onset influenced three different features of the response: amplitude of the AEP, high-gamma increase and alpha decrease (see Methods). We computed the weighted ITPC for each SEEG-IC, estimating their significance at the single level (permutation test). In only 2/60 oscillatory SEEG-ICs and 3/47 evoked SEEG-ICs, the phase of alpha oscillations influenced the intensity of the power response, either in the alpha or high-gamma range (Supplementary Figure 4). This indicates a marginal influence of alpha phase on

the power response. For the amplitude of the AEP, 15/46 evoked sources did present a significant link with the instantaneous phase of alpha, although this effect was not significant at the group level.

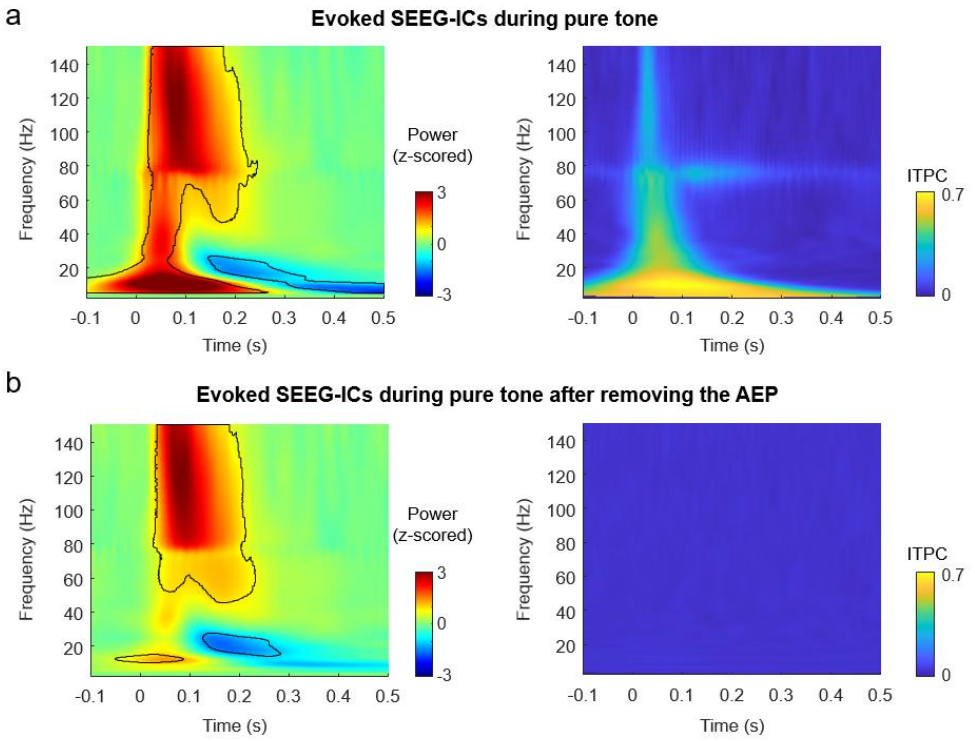

Figure 5: Time-frequency and phase locking responses of evoked SEEG-ICs:

a) Averaged time-frequency response of evoked SEEG-ICs during pure tone stimulation (left panel). Framed areas represent clusters of significant modulation of activity compared to baseline (-300 -200 ms; $p<0.01$, surrogate test). Inter-trial phase clustering (ITPC) representing the frequencies phase-locked with the stimulus (right panel)

b) Same analysis as in panel a but after removing the contribution of the averaged AEP to the evoked SEEG-IC time-courses. This process removes only the activity phase-locked with the stimulus.

Then, we compared the differences in the time-frequency activation between oscillatory and evoked sources (unpaired t-tests, corrected with FDR; Figure 6a). The high-gamma (80-120 Hz) response after stimulus onset (10-200 ms) was significantly higher in the evoked sources compared to the oscillatory sources ($p<0.05$, corrected with FDR). The short-lived low frequency (< 15 Hz) early response was also significantly stronger in the evoked sources. Note that this response does not coincide in time with the alpha suppression identified in Figures 3e and 5b (which is not significantly different across sources) and instead coincides in time with the

evoked potential. The low-gamma response (~20-40 Hz) also identified between 100 and 200 ms after stimulus onset was significantly higher in the oscillatory sources.

Finally, we tested whether the activation time between oscillatory and evoked sources differ during pure tone stimulation. We measured the evoked-related power at high-gamma (80-120 Hz) frequencies (Figure 6b) and measured the onset latency of this activity. Evoked sources responded significantly faster than oscillatory sources (68 ± 41 ms and 33 ± 24 ms for oscillatory and evoked SEEG-ICs, respectively; t-test, $p<0.0001$, $t=4.71$, $df=77$, CI=20, 50).

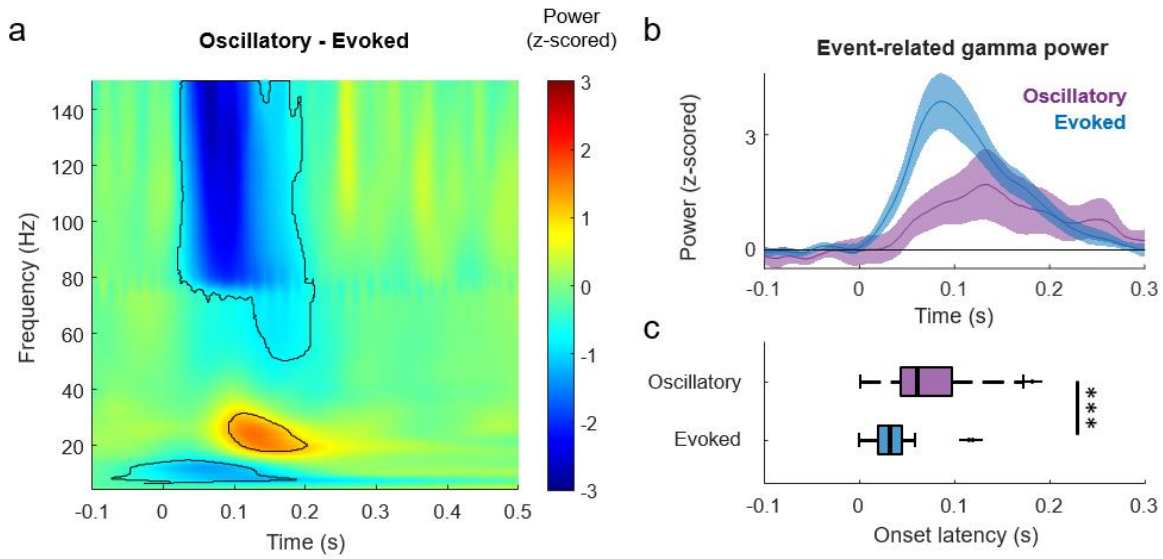

Figure 6: Comparison of the time-frequency dynamics between oscillatory and evoked SEEG-ICs

a) Contrast between the time-frequency responses of oscillatory (Figure 3e) minus evoked (Figure 5b) sources. Delineated areas represent the clusters with significant difference ($p<0.05$ corrected with FDR).
b) Averaged gamma power during pure tone stimulation of oscillatory and evoked SEEG-ICs (mean ± s.e.m.).
c) Onset latency of gamma activity for each source type. Evoked sources had a significant early activation than oscillatory SEEG-ICs suggesting a processing hierarchy.

DISCUSSION

In this work, we have identified two distinct type of activity sources in the auditory cortex: one presenting high alpha-like oscillations (5-10 Hz) during rest that are suppressed during auditory stimulation (oscillatory sources); and a second one that is relatively silent at rest but presents a significant evoked response during pure-tone stimulation (evoked sources). Results show that these sources are spatially segregated: the evoked source dominates in medial, primary auditory areas, while the oscillatory source is more distributed including lateral higher-level auditory regions (Figure 2). Both sources present a canonical time-frequency response to auditory stimulation, with a strong increase in high-gamma activity (80-120 Hz) followed by a decrease in the low-frequency range (5-30 Hz). A second decrease was also identified in the oscillatory sources in the alpha range (8 Hz). Unlike the transient effects observed in the time-frequency analysis, this decrease was not stimulus-locked but sustained throughout the entire pure tone stimulation task, compared to the resting condition (Figure 3d). Finally, short-lived early responses were also observed, with a low-frequency (~10 Hz) increase of activity in the evoked sources, characteristic of evoked responses, and a low-gamma (20-40 Hz) increase of activity in the oscillatory sources.

Evoked sources were activated progressively from medial to lateral areas (Figure 4b). This result, firstly reported in (Liégeois-Chauvel et al., 1994), is in line with the view of a hierarchical functional organization of the auditory cortex, where the information flows from primary to parabelt areas (Hickok and Poeppel, 2007). The onset latencies of the high-gamma response were also different between oscillatory and evoked sources (Figure 6c), with a faster response on the evoked SEEG-ICs (i.e., with a significant AEP). However, the correlation between activation time and location in the lateral-medial axis was relatively low, and it included lateral sources that were activated earlier in time (Figure 4b). Therefore, although the strict serial model seems the main route to process information, our results indicate the presence of multiple branches of communication between subcortical and (medial and lateral) cortical structures (Dubarry et al., 2017; Hamilton et al., 2021; Nourski et al., 2014).

It has been suggested that the main role of alpha oscillations is to inhibit task-irrelevant regions, while a reduction of this rhythm would disinhibit the system to favor information

processing (Jensen and Mazaheri, 2010; Klimesch et al., 2007; Strauß et al., 2014). In time-frequency maps, this is typically characterized as an increase of the high-gamma activity (information processing) followed by a suppression of the alpha activity (disinhibition) in regions engaged in the task (Edwards et al., 2009). In good agreement with previous studies (Billig et al., 2019; Nourski et al., 2022), we found that the high-gamma activity was dissociated from the alpha response, being stronger in the evoked sources (Figure 6a), mainly located in primary medial areas. There were no significant differences in alpha depression between evoked and oscillatory sources at the main timing of this effect (200-500 ms), suggesting that the amplitude of early high-gamma activity is not directly related to the amount of decrease of the alpha rhythm. Our results support the hypothesis of the stimulus-induced alpha suppression as a local bottom-up response to selectively engage the source to process the stimulus (Jia et al., 2022).

In addition to the induced alpha, we identified a sustained suppression of alpha oscillations during stimuli presentation (Figure 3). This spontaneous rhythm has been described as an active suppression mechanism of cortical synchronization (Weisz et al., 2011). During the presentation of pure tones this rhythm is strongly suppressed, facilitating the processing of the new sensory input. Given the basic nature of the stimuli and the task (passively listening to pure tones), together with the huge effect on the alpha power, our results suggests that the main goal of this sustained alpha suppression in the auditory cortex is to facilitate the processing of every acoustic information, while smaller changes induced by the stimulus may represent a bottom-up process to attract attention (Foxe and Snyder, 2011) or to modulate the complexity of the stimuli (Obleser and Weisz, 2012).

It has been described a gradient in alpha power in the auditory cortex (Billig et al., 2019). Compared to posteromedial structures, anterolateral areas have higher levels of alpha activity before auditory stimulation, followed by a stronger alpha suppression in response to sentences. Our work complements this result by describing two types of alpha suppression (sustained and induced). The evoked sources, mainly related to primary posteromedial structures, presented low alpha power during rest. The oscillatory sources, more distributed and covering lateral areas, were characterized by large alpha oscillations, corroborating the results reported before stimulus onset (Billig et al., 2019). While the induced alpha suppression in response to pure

tones was similar for both sources (Figure 6a), the strong sustained alpha suppression, only present in oscillatory sources, may align with the identified gradient (Billig et al., 2019). As the time interval between sentences in (Billig et al., 2019) was up to several seconds, it is possible that the auditory system had enough time to recover and reestablish the alpha power to a level similar to the resting condition.

It is worthy at this point to comment on the "oscillatory" nature of alpha. It has been suggested that the alpha cycle imposes the "opportunity windows" or "duty-cycle" of gamma activity (Jensen et al., 2014). However, our results suggest that the changes in alpha oscillations, defined as a sustained suppression in the oscillatory sources, may not be related with the induced alpha activity, given that both phenomena can be dissociated. In this scenario, we would have two systems: a sustained oscillatory alpha rhythm whose phase and amplitude are determinant of the inhibitory state of the network (Osipova et al., 2008; Voytek et al., 2010), and an alpha activity (not necessary an oscillation), whose suppression indexes the facilitation of information flow after stimulus onset. Whether both systems are related or not is a question that needs to be answered.

The suppression of the alpha activity found in our study cannot be accounted by changes in the $1/f^x$ component of the power spectrum as our methodology separated the oscillatory and aperiodic components (Donoghue et al., 2020). Nevertheless, we also identified a decrease in the slope of the signal during pure tones in both sources (Billig et al., 2019). This difference could be explained by a global increase in neural activity during the task (Podvalny et al., 2015) and may be linked to an increase in the excitation/inhibition balance of the network (Voytek and Knight, 2015).

Two additional differences were identified when comparing the time-frequency map of the sources (Figure 6a). A low-gamma (20-40 Hz) early response was present in the oscillatory sources, but not in the evoked ones. While this response may be related to the temporal duration of the pure tone stimulus (30 ms), its absence in the evoked sources (associated to primary areas and to stimulus response) is striking. One possibility is that the oscillatory sources have a higher sensitivity to stimuli with a low-gamma period (Giroud et al., 2020; Morillon et al.,

2012; Teng and Poeppel, 2020), a key frequency for phonemic processing (Marchesotti et al., 2020) that becomes left-lateralized in more associative (anterior STG; A4) regions (Giroud et al., 2020; Morillon et al., 2010). A low-frequency short-lived early response was also specifically present in the evoked sources, which corresponds to the typical spectral signature of an AEP and would hence be caused by presence of vestiges of the AEP.

One limitation of our work is the categorical differentiation between sources. While oscillatory and evoked sources can be identified and separated, the former exhibits an evoked response in the time-frequency plane (Figure 3e) and the latter show an alpha peak in the spectrum (Figure 4d), suggesting that both phenomena are not completely dissociated. Therefore, the anatomical segregation in Figure 2 could reflect a gradual change of alpha dominance. We did not observe any anatomical gradient of alpha power (Supplementary Figure 2), supporting our hypothesis of two independent sources in the auditory cortex.

While we focus our work on alpha oscillations, these are not the only rhythms in the auditory cortex (Mai et al., 2016). For instance, theta (4-8 Hz) and delta (0-4 Hz) oscillations are key dynamics for speech processing, with the former tracking the syllabic time scale (Luo and Poeppel, 2007) and the latter associated with prosody (Inbar et al., 2023), pauses (Chalas et al., 2023) and other top-down (Fontolan et al., 2014) or linguistic processes (Chalas et al., 2024). Given the nature of our stimuli (short pure tones) and the short intertrial interval (~1s), these oscillations are beyond the scope and possibilities of this study. Further work should investigate the interaction between alpha and other brain oscillations, and particularly explore whether, in continuous stimulation contexts such as speech or music perception, the gating of information depends on contextual or predictive features.

Another general limitation inherent to every intracerebral study is the diagnosis of epilepsy. Although it cannot be fully addressed, several precautions can be taken to mitigate its impact. Every trace of epileptic activity was excluded from the analysis, and a partial or complete withdrawal of antiepileptic drug is done prior to the beginning of SEEG exploration, and none of the patients had their epileptogenic zone including the auditory areas. However, functional changes have been detected even in regions non-involved in the epileptic network

(Lagarde et al., 2018). While they mainly affect the broadband connectivity between regions (not studied in this work), we cannot completely rule out any effect in alpha oscillations.

Overall, based on our results we can hypothesize that primary auditory areas have a generally disinhibited state without resting oscillations, ready to process any new stimulus, while there is an inhibitory alpha oscillation who gates or not the information to high-level structures. Both evoked and oscillatory sources have a local bottom-up inhibitory system that becomes active after receiving a new input (induced alpha). Oscillatory sources would have a general inhibitory system that would be steadily suppressed when expecting or processing new information. This sustained suppression also includes the preparatory phase of the task (Müller and Weisz, 2012), indicating a top-down anticipatory disinhibition prior the stimulus. Finally, the weak high-gamma response and lack of evoked potentials in the oscillatory sources suggests that the sustained alpha rhythm is not restricted to a local inhibition (Weisz et al., 2011) but belongs to a larger network, encompassing primary and non-primary auditory areas.

ACKNOWLEDGEMENTS

We would like to thank Manuel Mercier for assisting with the data collection and the development of the computational framework for localizing the SEEG electrodes in common patient space, Paul Lalande-Robert for his help on the visualization of the results and Aurélie Bidet-Caulet for helping with the interpretation of the results. This study was supported by a postdoctoral fellowship from the Institute of Language, Cognition and the Brain (ILCB, grant ANR-16-CONV-0002). This work has received support from the ANR-20-CE28-0007-01 (to B.M), ANR-21-CE28-0010 (to D.S), ANR-17-EURE-0029 (NeuroMarseille), Fondation Pour l'Audition (FPA RD-2022-09), and co-funded by the European Union (ERC, SPEEDY, ERC-CoG-101043344). It was also supported by the French government under the Programme «Investissements d'Avenir», and the Excellence Initiative of Aix-Marseille University (A*MIDEX, AMX-19-IET-004).

AUTHOR CONTRIBUTIONS

All authors Designed Research; VLM, AT, BM Performed Research; VLM Analyzed Data; VLM, DS, BM Interpreted results; VLM Wrote the first draft of the paper; all authors Contributed to the manuscript final writing.

BIBLIOGRAPHY

Ahveninen, J., Lee, H.-J., Yu, H.-Y., Lee, C.-C., Chou, C.-C., Ahlfors, S.P., Kuo, W.-J., Jääskeläinen, I.P., Lin, F.-H., 2024. Visual Stimuli Modulate Local Field Potentials But Drive No High-Frequency Activity in Human Auditory Cortex. J. Neurosci. 44. https://doi.org/10.1523/JNEUROSCI.0890-23.2023

Armonaite, K., Bertoli, M., Paulon, L., Gianni, E., Balsi, M., Conti, L., Tecchio, F., 2022. Neuronal Electrical Ongoing Activity as Cortical Areas Signature: An Insight from MNI Intracerebral Recording Atlas. Cereb. Cortex 32, 2895–2906. https://doi.org/10.1093/cercor/bhab389

Artoni, F., Delorme, A., Makeig, S., 2018. Applying dimension reduction to EEG data by Principal Component Analysis reduces the quality of its subsequent Independent Component decomposition. NeuroImage 175, 176–187. https://doi.org/10.1016/j.neuroimage.2018.03.016

Bell, A.J., Sejnowski, T.J., 1995. An information-maximization approach to blind separation and blind deconvolution. Neural Comput. 7, 1129–1159. https://doi.org/10.1162/neco.1995.7.6.1129

Billig, A.J., Herrmann, B., Rhone, A.E., Gander, P.E., Nourski, K.V., Snoad, B.F., Kovach, C.K., Kawasaki, H., Howard, M.A., Johnsrude, I.S., 2019. A Sound-Sensitive Source of Alpha Oscillations in Human Non-Primary Auditory Cortex. J. Neurosci. 39, 8679–8689. https://doi.org/10.1523/JNEUROSCI.0696-19.2019

Buzsaki, G., 2011. Rhythms of the Brain, 1er édition. ed. Oxford University Press, U.S.A., Oxford ; New York.

Capilla, A., Arana, L., García-Huéscar, M., Melcón, M., Gross, J., Campo, P., 2022. The natural frequencies of the resting human brain: An MEG-based atlas. NeuroImage 258, 119373. https://doi.org/10.1016/j.neuroimage.2022.119373

Chalas, N., Daube, C., Kluger, D.S., Abbasi, O., Nitsch, R., Gross, J., 2023. Speech onsets and sustained speech contribute differentially to delta and theta speech tracking in auditory cortex. Cereb. Cortex 33, 6273–6281. https://doi.org/10.1093/cercor/bhac502

Chalas, N., Meyer, L., Lo, C.-W., Park, H., Kluger, D.S., Abbasi, O., Kayser, C., Nitsch, R., Gross, J., 2024. Dissociating prosodic from syntactic delta activity during natural speech comprehension. Curr. Biol. 34, 3537-3549.e5. https://doi.org/10.1016/j.cub.2024.06.072

Chaumon, M., Busch, N.A., 2014. Prestimulus neural oscillations inhibit visual perception via modulation of response gain. J. Cogn. Neurosci. 26, 2514–2529. https://doi.org/10.1162/jocn_a_00653

Cohen, M.X., 2014. Analyzing Neural Time Series Data: Theory and Practice. MIT Press.

Collins, D.L., Neelin, P., Peters, T.M., Evans, A.C., 1994. Automatic 3D intersubject registration of MR volumetric data in standardized Talairach space. J. Comput. Assist. Tomogr. 18, 192–205.

Delorme, A., Makeig, S., 2004. EEGLAB: an open source toolbox for analysis of single-trial EEG dynamics including independent component analysis. J. Neurosci. Methods 134, 9–21. https://doi.org/10.1016/j.jneumeth.2003.10.009

Donoghue, T., Haller, M., Peterson, E.J., Varma, P., Sebastian, P., Gao, R., Noto, T., Lara, A.H., Wallis, J.D., Knight, R.T., Shestyuk, A., Voytek, B., 2020. Parameterizing neural power spectra into periodic and aperiodic components. Nat. Neurosci. 23, 1655–1665. https://doi.org/10.1038/s41593-020-00744-x

Dubarry, A.-S., Llorens, A., Trébuchon, A., Carron, R., Liégeois-Chauvel, C., Bénar, C.-G., Alario, F.-X., 2017. Estimating Parallel Processing in a Language Task Using Single-Trial Intracerebral Electroencephalography. Psychol. Sci. 28, 414–426. https://doi.org/10.1177/0956797616681296

Edwards, E., Soltani, M., Kim, W., Dalal, S.S., Nagarajan, S.S., Berger, M.S., Knight, R.T., 2009. Comparison of time-frequency responses and the event-related potential to auditory speech stimuli in human cortex. J. Neurophysiol. 102, 377–386. https://doi.org/10.1152/jn.90954.2008

ElShafei, H.A., Fornoni, L., Masson, R., Bertrand, O., Bidet-Caulet, A., 2020. Age-related modulations of alpha and gamma brain activities underlying anticipation and distraction. PLOS ONE 15, e0229334. https://doi.org/10.1371/journal.pone.0229334

Fan, L., Li, H., Zhuo, J., Zhang, Y., Wang, J., Chen, L., Yang, Z., Chu, C., Xie, S., Laird, A.R., Fox, P.T., Eickhoff, S.B., Yu, C., Jiang, T., 2016. The Human Brainnetome Atlas: A New Brain Atlas Based on Connectional Architecture. Cereb. Cortex N. Y. NY 26, 3508–3526. https://doi.org/10.1093/cercor/bhw157

Fernández-Ruiz, A., Herreras, O., 2013. Identifying the synaptic origin of ongoing neuronal oscillations through spatial discrimination of electric fields. Front. Comput. Neurosci. 7, 5. https://doi.org/10.3389/fncom.2013.00005

Fontolan, L., Morillon, B., Liegeois-Chauvel, C., Giraud, A.-L., 2014. The contribution of frequency-specific activity to hierarchical information processing in the human auditory cortex. Nat. Commun. 5, 4694. https://doi.org/10.1038/ncomms5694

Foxe, J., Snyder, A., 2011. The Role of Alpha-Band Brain Oscillations as a Sensory Suppression Mechanism during Selective Attention. Front. Psychol. 2.

Frauscher, B., von Ellenrieder, N., Zelmann, R., Doležalová, I., Minotti, L., Olivier, A., Hall, J., Hoffmann, D., Nguyen, D.K., Kahane, P., Dubeau, F., Gotman, J., 2018. Atlas of the normal intracranial electroencephalogram: neurophysiological awake activity in different cortical areas. Brain J. Neurol. 141, 1130–1144. https://doi.org/10.1093/brain/awy035

Giroud, J., Trébuchon, A., Schön, D., Marquis, P., Liegeois-Chauvel, C., Poeppel, D., Morillon, B., 2020. Asymmetric sampling in human auditory cortex reveals spectral processing hierarchy. PLoS Biol. 18, e3000207. https://doi.org/10.1371/journal.pbio.3000207

Groppe, D.M., Bickel, S., Keller, C.J., Jain, S.K., Hwang, S.T., Harden, C., Mehta, A.D., 2013. Dominant frequencies of resting human brain activity as measured by the electrocorticogram. NeuroImage 79, 223–233. https://doi.org/10.1016/j.neuroimage.2013.04.044

Hamilton, L.S., Oganian, Y., Hall, J., Chang, E.F., 2021. Parallel and distributed encoding of speech across human auditory cortex. Cell 184, 4626-4639.e13. https://doi.org/10.1016/j.cell.2021.07.019

Herreras, O., Makarova, J., Makarov, V.A., 2015. New uses of LFPs: Pathway-specific threads obtained through spatial discrimination. Neuroscience 310, 486–503. https://doi.org/10.1016/j.neuroscience.2015.09.054

Herreras, O., Torres, D., Martín-Vázquez, G., Hernández-Recio, S., López-Madrona, V.J., Benito, N., Makarov, V.A., Makarova, J., 2022. Site-dependent shaping of field potential waveforms. Cereb. Cortex bhac297. https://doi.org/10.1093/cercor/bhac297

Hickok, G., Poeppel, D., 2007. The cortical organization of speech processing. Nat. Rev. Neurosci. 8, 393–402. https://doi.org/10.1038/nrn2113

Hu, S., Stead, M., Worrell, G.A., 2007. Automatic identification and removal of scalp reference signal for intracranial EEGs based on independent component analysis. IEEE Trans. Biomed. Eng. 54, 1560–1572. https://doi.org/10.1109/TBME.2007.892929

Inbar, M., Genzer, S., Perry, A., Grossman, E., Landau, A.N., 2023. Intonation Units in Spontaneous Speech Evoke a Neural Response. J. Neurosci. 43, 8189–8200. https://doi.org/10.1523/JNEUROSCI.0235-23.2023

Jensen, O., Gips, B., Bergmann, T.O., Bonnefond, M., 2014. Temporal coding organized by coupled alpha and gamma oscillations prioritize visual processing. Trends Neurosci. 37, 357–369. https://doi.org/10.1016/j.tins.2014.04.001

Jensen, O., Mazaheri, A., 2010. Shaping Functional Architecture by Oscillatory Alpha Activity: Gating by Inhibition. Front. Hum. Neurosci. 4.

Jia, J., Fan, Y., Luo, H., 2022. Alpha-Band Phase Modulates Bottom-up Feature Processing. Cereb. Cortex 32, 1260–1268. https://doi.org/10.1093/cercor/bhab291

Jung, T.P., Makeig, S., Humphries, C., Lee, T.W., McKeown, M.J., Iragui, V., Sejnowski, T.J., 2000. Removing electroencephalographic artifacts by blind source separation. Psychophysiology 37, 163–178.

Klimesch, W., 2012. Alpha-band oscillations, attention, and controlled access to stored information. Trends Cogn. Sci. 16, 606–617. https://doi.org/10.1016/j.tics.2012.10.007

Klimesch, W., Sauseng, P., Hanslmayr, S., 2007. EEG alpha oscillations: the inhibition-timing hypothesis. Brain Res. Rev. 53, 63–88. https://doi.org/10.1016/j.brainresrev.2006.06.003

Krieg, J., Trébuchon-Da Fonseca, A., Martínez-Montes, E., Marquis, P., Liégeois-Chauvel, C., Bénar, C.-G., 2011. A comparison of methods for assessing alpha phase resetting in electrophysiology, with application to intracerebral EEG in visual areas. NeuroImage 55, 67–86. https://doi.org/10.1016/j.neuroimage.2010.11.058

Lagarde, S., Roehri, N., Lambert, I., Trebuchon, A., McGonigal, A., Carron, R., Scavarda, D., Milh, M., Pizzo, F., Colombet, B., Giusiano, B., Medina Villalon, S., Guye, M., Bénar, C.-G., Bartolomei, F., 2018. Interictal stereotactic-EEG functional connectivity in refractory focal epilepsies. Brain 141, 2966–2980. https://doi.org/10.1093/brain/awy214

Lehtelä, L., Salmelin, R., Hari, R., 1997. Evidence for reactive magnetic 10-Hz rhythm in the human auditory cortex. Neurosci. Lett. 222, 111–114. https://doi.org/10.1016/S0304-3940(97)13361-4

Liégeois-Chauvel, C., Musolino, A., Badier, J.M., Marquis, P., Chauvel, P., 1994. Evoked potentials recorded from the auditory cortex in man: evaluation and topography of the middle latency components. Electroencephalogr. Clin. Neurophysiol. Potentials Sect. 92, 204–214. https://doi.org/10.1016/0168-5597(94)90064-7

López-Madrona, V.J., Medina Villalon, S., Badier, J.-M., Trébuchon, A., Jayabal, V., Bartolomei, F., Carron, R., Barborica, A., Vulliémoz, S., Alario, F.-X., Bénar, C.G., 2022. Magnetoencephalography can reveal deep brain network activities linked to memory processes. Hum. Brain Mapp. 43, 4733–4749. https://doi.org/10.1002/hbm.25987

López-Madrona, V.J., Trébuchon, A., Mindruta, I., Barbeau, E.J., Barborica, A., Pistol, C., Oane, I., Alario, F.X., Bénar, C.G., 2024. Identification of early hippocampal dynamics during recognition memory with independent component analysis. eNeuro 11. https://doi.org/10.1523/ENEURO.0183-23.2023

López-Madrona, V.J., Villalon, S.M., Velmurugan, J., Semeux-Bernier, A., Garnier, E., Badier, J.-M., Schön, D., Bénar, C.-G., 2023. Reconstruction and localization of auditory sources from intracerebral SEEG using independent component analysis. NeuroImage 269, 119905. https://doi.org/10.1016/j.neuroimage.2023.119905

Luo, H., Poeppel, D., 2007. Phase Patterns of Neuronal Responses Reliably Discriminate Speech in Human Auditory Cortex. Neuron 54, 1001–1010. https://doi.org/10.1016/j.neuron.2007.06.004

Mai, G., Minett, J.W., Wang, W.S.-Y., 2016. Delta, theta, beta, and gamma brain oscillations index levels of auditory sentence processing. NeuroImage 133, 516–528. https://doi.org/10.1016/j.neuroimage.2016.02.064

Makarov, V.A., Makarova, J., Herreras, O., 2010. Disentanglement of local field potential sources by independent component analysis. J. Comput. Neurosci. 29, 445–457. https://doi.org/10.1007/s10827-009-0206-y

Marchesotti, S., Nicolle, J., Merlet, I., Arnal, L.H., Donoghue, J.P., Giraud, A.-L., 2020. Selective enhancement of low-gamma activity by tACS improves phonemic processing and reading accuracy in dyslexia. PLoS Biol. 18, e3000833. https://doi.org/10.1371/journal.pbio.3000833

Maris, E., Oostenveld, R., 2007. Nonparametric statistical testing of EEG- and MEG-data. J. Neurosci. Methods 164, 177–190. https://doi.org/10.1016/j.jneumeth.2007.03.024

Martín-Vázquez, G., Makarova, J., Makarov, V.A., Herreras, O., 2013. Determining the true polarity and amplitude of synaptic currents underlying gamma oscillations of local field potentials. PloS One 8, e75499. https://doi.org/10.1371/journal.pone.0075499

Medina Villalon, S., Makhalova, J., López-Madrona, V.J., Garnier, E., Badier, J.-M., Bartolomei, F., Bénar, C.G., 2024. Combining independent component analysis and source localization for improving spatial sampling of stereoelectroencephalography in epilepsy. Sci. Rep. 14, 4071. https://doi.org/10.1038/s41598-024-54359-4

Medina Villalon, S., Paz, R., Roehri, N., Lagarde, S., Pizzo, F., Colombet, B., Bartolomei, F., Carron, R., Bénar, C.-G., 2018. EpiTools, A software suite for presurgical brain mapping in epilepsy: Intracerebral EEG. J. Neurosci. Methods 303, 7–15. https://doi.org/10.1016/j.jneumeth.2018.03.018

Michelmann, S., Treder, M.S., Griffiths, B., Kerrén, C., Roux, F., Wimber, M., Rollings, D., Sawlani, V., Chelvarajah, R., Gollwitzer, S., Kreiselmeyer, G., Hamer, H., Bowman, H., Staresina, B., Hanslmayr, S., 2018. Data-driven re-referencing of intracranial EEG based on independent component analysis (ICA). J. Neurosci. Methods 307, 125–137. https://doi.org/10.1016/j.jneumeth.2018.06.021

Morillon, B., Lehongre, K., Frackowiak, R.S.J., Ducorps, A., Kleinschmidt, A., Poeppel, D., Giraud, A.-L., 2010. Neurophysiological origin of human brain asymmetry for speech and language. Proc. Natl. Acad. Sci. U. S. A. 107, 18688–18693. https://doi.org/10.1073/pnas.1007189107

Morillon, B., Liégeois-Chauvel, C., Arnal, L.H., Bénar, C.-G., Giraud, A.-L., 2012. Asymmetric Function of Theta and Gamma Activity in Syllable Processing: An Intra-Cortical Study. Front. Psychol. 3. https://doi.org/10.3389/fpsyg.2012.00248

Morosan, P., Rademacher, J., Schleicher, A., Amunts, K., Schormann, T., Zilles, K., 2001. Human Primary Auditory Cortex: Cytoarchitectonic Subdivisions and Mapping into a Spatial Reference System. NeuroImage 13, 684–701. https://doi.org/10.1006/nimg.2000.0715

Müller, N., Weisz, N., 2012. Lateralized Auditory Cortical Alpha Band Activity and Interregional Connectivity Pattern Reflect Anticipation of Target Sounds. Cereb. Cortex 22, 1604–1613. https://doi.org/10.1093/cercor/bhr232

Neymotin, S.A., Tal, I., Barczak, A., O'Connell, M.N., McGinnis, T., Markowitz, N., Espinal, E., Griffith, E., Anwar, H., Dura-Bernal, S., Schroeder, C.E., Lytton, W.W., Jones, S.R., Bickel, S., Lakatos, P., 2022. Detecting Spontaneous Neural Oscillation Events in Primate Auditory Cortex. eNeuro 9. https://doi.org/10.1523/ENEURO.0281-21.2022

Nourski, K.V., Steinschneider, M., McMurray, B., Kovach, C.K., Oya, H., Kawasaki, H., Howard, M.A., 2014. Functional organization of human auditory cortex: investigation of response latencies through direct recordings. NeuroImage 101, 598–609. https://doi.org/10.1016/j.neuroimage.2014.07.004

Nourski, K.V., Steinschneider, M., Rhone, A.E., Kovach, C.K., Kawasaki, H., Howard, M.A., 2022. Gamma Activation and Alpha Suppression within Human Auditory Cortex during a Speech Classification Task. J. Neurosci. 42, 5034–5046. https://doi.org/10.1523/JNEUROSCI.2187-21.2022

Obleser, J., Weisz, N., 2012. Suppressed Alpha Oscillations Predict Intelligibility of Speech and its Acoustic Details. Cereb. Cortex 22, 2466–2477. https://doi.org/10.1093/cercor/bhr325

Oostenveld, R., Fries, P., Maris, E., Schoffelen, J.-M., 2011. FieldTrip: Open source software for advanced analysis of MEG, EEG, and invasive electrophysiological data. Comput. Intell. Neurosci. 2011, 156869. https://doi.org/10.1155/2011/156869

Osipova, D., Hermes, D., Jensen, O., 2008. Gamma Power Is Phase-Locked to Posterior Alpha Activity. PLOS ONE 3, e3990. https://doi.org/10.1371/journal.pone.0003990

Phipson, B., Smyth, G.K., 2010. Permutation P-values Should Never Be Zero: Calculating Exact P-values When Permutations Are Randomly Drawn. Stat. Appl. Genet. Mol. Biol. 9. https://doi.org/10.2202/1544-6115.1585

Podvalny, E., Noy, N., Harel, M., Bickel, S., Chechik, G., Schroeder, C.E., Mehta, A.D., Tsodyks, M., Malach, R., 2015. A unifying principle underlying the extracellular field potential spectral responses in the human cortex. J. Neurophysiol. 114, 505–519. https://doi.org/10.1152/jn.00943.2014

Schroeder, C.E., Lakatos, P., Kajikawa, Y., Partan, S., Puce, A., 2008. Neuronal oscillations and visual amplification of speech. Trends Cogn. Sci. 12, 106–113. https://doi.org/10.1016/j.tics.2008.01.002

Strauß, A., Wöstmann, M., Obleser, J., 2014. Cortical alpha oscillations as a tool for auditory selective inhibition. Front. Hum. Neurosci. 8. https://doi.org/10.3389/fnhum.2014.00350

Talairach, J., Tournoux, P., Musolino, A., Missir, O., 1992. Stereotaxic exploration in frontal epilepsy. Adv. Neurol. 57, 651–688.

Teng, X., Poeppel, D., 2020. Theta and Gamma Bands Encode Acoustic Dynamics over Wide-Ranging Timescales. Cereb. Cortex N. Y. N 1991 30, 2600–2614. https://doi.org/10.1093/cercor/bhz263

Thézé, R., Giraud, A.-L., Mégevand, P., 2020. The phase of cortical oscillations determines the perceptual fate of visual cues in naturalistic audiovisual speech. Sci. Adv. 6, eabc6348. https://doi.org/10.1126/sciadv.abc6348

Thomson, D.J., 1982. Spectrum estimation and harmonic analysis. Proc. IEEE 70, 1055–1096. https://doi.org/10.1109/PROC.1982.12433

Thut, G., Miniussi, C., Gross, J., 2012. The Functional Importance of Rhythmic Activity in the Brain. Curr. Biol. 22, R658–R663. https://doi.org/10.1016/j.cub.2012.06.061

Tiihonen, J., Hari, R., Kajola, M., Karhu, J., Ahlfors, S., Tissari, S., 1991. Magnetoencephalographic 10-Hz rhythm from the human auditory cortex. Neurosci. Lett. 129, 303–305. https://doi.org/10.1016/0304-3940(91)90486-D

Velmurugan, J., Badier, J.-M., Pizzo, F., Medina Villalon, S., Papageorgakis, C., López-Madrona, V., Jegou, A., Carron, R., Bartolomei, F., Bénar, C.-G., 2022. Virtual MEG sensors based on beamformer and independent component analysis can reconstruct epileptic activity as measured on simultaneous intracerebral recordings. NeuroImage 264, 119681. https://doi.org/10.1016/j.neuroimage.2022.119681

Voytek, B., Canolty, R.T., Shestyuk, A., Crone, N.E., Parvizi, J., Knight, R.T., 2010. Shifts in gamma phase-amplitude coupling frequency from theta to alpha over posterior cortex during visual tasks. Front. Hum. Neurosci. 4, 191. https://doi.org/10.3389/fnhum.2010.00191

Voytek, B., Knight, R.T., 2015. Dynamic network communication as a unifying neural basis for cognition, development, aging, and disease. Biol. Psychiatry 77, 1089–1097. https://doi.org/10.1016/j.biopsych.2015.04.016

Voytek, B., Kramer, M.A., Case, J., Lepage, K.Q., Tempesta, Z.R., Knight, R.T., Gazzaley, A., 2015. Age-Related Changes in 1/f Neural Electrophysiological Noise. J. Neurosci. 35, 13257–13265. https://doi.org/10.1523/JNEUROSCI.2332-14.2015

Weisz, N., Hartmann, T., Müller, N., Obleser, J., 2011. Alpha Rhythms in Audition: Cognitive and Clinical Perspectives. Front. Psychol. 2.

Whitmore, N.W., Lin, S.-C., 2016. Unmasking local activity within local field potentials (LFPs) by removing distal electrical signals using independent component analysis. NeuroImage 132, 79–92. https://doi.org/10.1016/j.neuroimage.2016.02.032

SUPPLEMENTARY MATERIAL

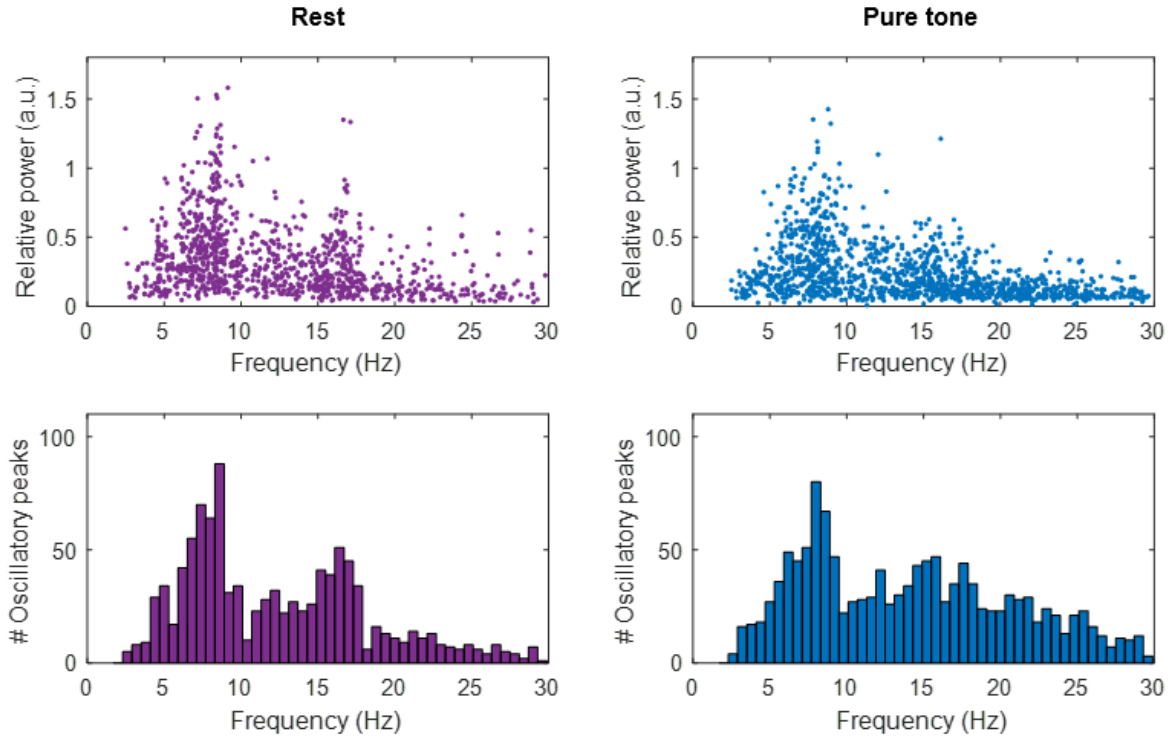

Supplementary Figure 1:

Distribution of peaks identified with the fooof approach for all the SEEG-ICs. There are two clear clusters of peaks, centered around 8 Hz and its first harmonic 16 Hz. The most prominent oscillations (i.e., peaks with higher relative power) were also centered between 5 and 10 Hz.

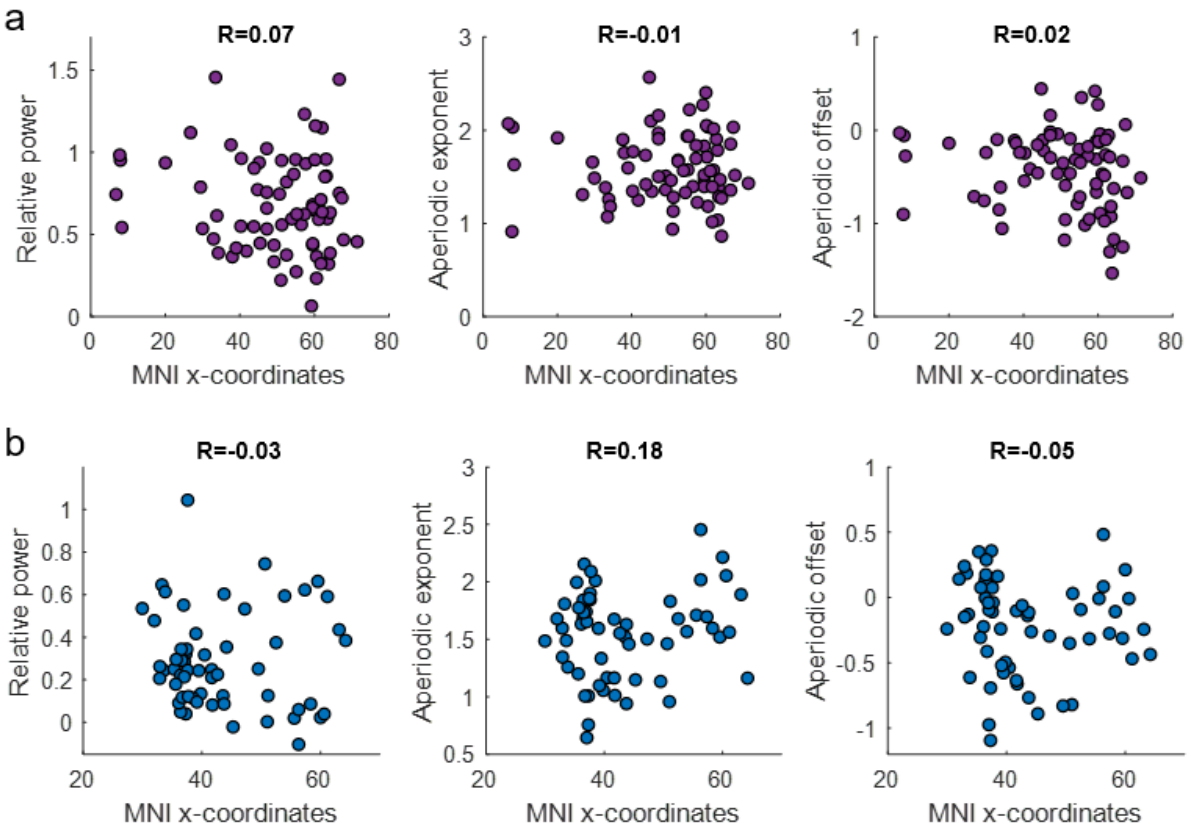

Supplementary Figure 2:

(a) Correlation between location of the oscillatory sources (position in the lateral-medial axis) and the main spectral features obtained from the fooof analysis: the relative power of the main oscillatory activity, the exponent and the offset of the aperiodic component. No significant correlations were found.

(b) Correlation between location of the evoked sources and the main spectral features.

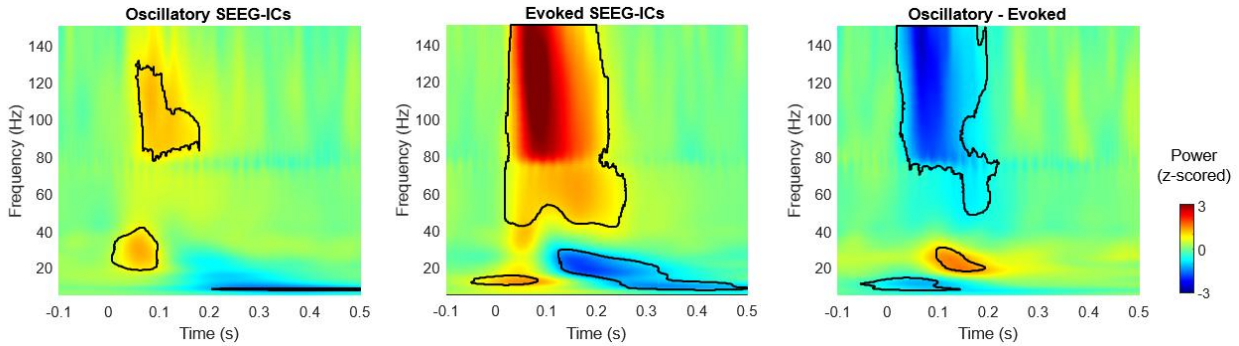

Supplementary Figure 3: Time-frequency response across patients during pure tone stimulation for oscillatory sources (left), evoked sources (middle) and difference between oscillatory and evoked sources. For patients with multiple oscillatory or evoked SEEG-ICs, we averaged them to have a single oscillatory and evoked source per subject. For left and middle panels, framed areas represent clusters of significant modulation of activity compared to baseline (-300 -200 ms, $p<0.01$, surrogate test, N=20). For right panel, delineated areas represent the clusters with significant difference ($p<0.05$ corrected with FDR, N=20).

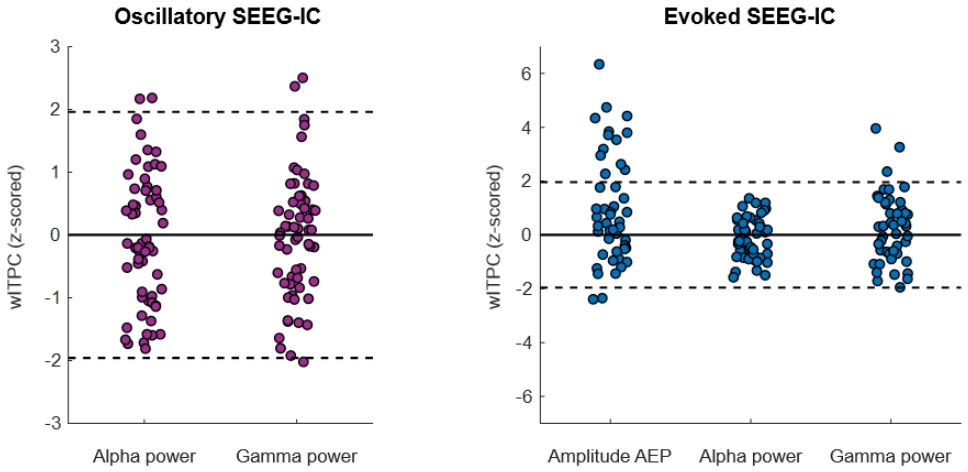

Supplementary Figure 4: Weighted ITPC between the instantaneous phase of alpha oscillations at stimulus arrival and three different features of the response: alpha (5-10 Hz) power, high-gamma (80-120 Hz) power and amplitude of the AEP. Each point represents one SEEG-IC. Dashed lines correspond to the significant threshold, stablished at 1.96. Values outside this rage were considered as significant.